

International airport emissions and their impact on local air quality: Chemical speciation of ambient aerosols at Madrid-Barajas Airport during AVIATOR Campaign

Saleh Alzahrani¹, Doğuşan Kılıç^{1,2}, Michael Flynn¹, Paul I. Williams^{1,2} and James Allan^{1,2}

¹Department of Earth and Environmental Sciences, University of Manchester, Manchester, UK

²National Centre for Atmospheric Science, University of Manchester, Manchester, UK

Correspondence to: Saleh Alzahrani (Saleh.alzahrani@manchester.ac.uk)

Abstract. Madrid-Barajas International Airport (MAD), located in Spanish Capital Madrid, is the fourth-busiest airport in Europe. As part of the AVIATOR campaign, The aerosol chemical composition of particulate matter and other the concentrations of other key pollutants were measured at the airport perimeter during October 2021, to assess the impact of airport emissions on local air quality. A high-fidelity ambient instrumentation system was deployed at Madrid Airport to measure: concentrations of organic aerosols (with their composition), composition of ambient aerosol and concentrations of black carbon (eBC), carbon dioxide (CO₂), carbon monoxide (CO), nitrogen dioxide (NO_x), sulphur dioxide (SO₂), particulate matter (PM_{2.5}, PM₁₀), total hydrocarbon (THC), and total particle number. The average concentration for the entire campaign of eBC, NO_x, SO₂, PM_{2.5}, PM₁₀, CO and THC at the airport for the entire campaign were, 1.07 (µg/m³), 22.7 (µg/m³), 4.10 (µg/m³), 9.35 (µg/m³), 16.43 (µg/m³), 0.23 (mg/m³) and 2.30 (mg/m³) respectively. The source apportionment analysis of the non-refractory organic aerosol (OA) using positive matrix factorisation (PMF) allowed us to discriminate between different sources of pollution, namely: Less Oxidised Oxygenated Organic Aerosol (LO-OOA), Alkane Organic Aerosol (AlkOA), and More Oxidised Oxygenated Organic Aerosol (MO-OOA) source. The results showed that LO-OOA and MO-OOA accounts for more than 80% of the total organic particle mass that was measured near runway at the airport. Trace gases correlate better with AlkOA factor more than LO-OOA and MO-OOA which indicating that AlkOA is mainly related to the primary combustion emissions of combustion. Bivariate polar plots were used for the pollutant source identification. Significantly higher concentrations of the obtained factors were observed at low wind speeds (< 3m/s) from the southwest, where two of runways, as well as and all terminals are located. Higher SO₂/NO_x and CO/eBC ratios were observed when the winds originating from the northeast, where the two northern 18L/36R runways are located. This is These elevated ratios are attributed to the aircraft influence activity being the major source and the lack of a local road source in the northeast area.

1. Introduction

Several studies have linked particulate matter (PM) to a range of harmful health effects, including respiratory and cardiovascular ailments (Boldo et al., 2006; Li et al., 2003a; Pope and Dockery, 2006; Schwarze et al. et al., 2006). In recent years, a number of researchers have found an association between aviation emissions and potential adverse human health impacts. These emissions can lead to immune system malfunction, various pathologies, the development of cancer, and premature death. Hence, it is increasingly recognised as a serious, worldwide public health concern (Yim et al., 2013; He et al., 2018; Jonsdottir et al., 2019). Airports contribute to primary and secondary inhalable and fine particulate matter (PM₁₀ and PM_{2.5}, with aerodynamic diameters of <10 µm and <2.5 µm, respectively), making them key determinants of urban air quality and a significant concern for local air quality management. A few studies have reported that air pollutants emitted from large airports can play a vital role in worsening the regional air quality (Rissman et al., 2013; Hudda and Fruin, 2016). Hu et al., (2009) and Westerdahl et al., (2008) measured high ambient PM concentrations downwind of Los Angeles International Airport (LAX) and Santa Monica Airport (SMA) in California. A decline in the ambient air quality was observed over distances of up to 18 km downwind from international airports owing due to an increase in particle number concentrations linked to gas turbine-emitted PM (Hudda et al., 2014; Hudda and Fruin, 2016). Airports' contribution to primary and secondary inhalable and fine particulate matter (PM₁₀ and PM_{2.5}, mass of particles with aerodynamic diameters <10 µm and <2.5 µm, respectively) making them determinants of the air quality in cities and a significant issue for the local air quality management. To date, several questions still remain to be answered regarding the chemical composition of aircraft plumes, and the health risks associated with the exposure to the pollutants originating from

Formatted: Underline, Highlight

Formatted: Underline, Highlight

Formatted: Underline, Highlight

Formatted: Underline, Highlight

Formatted: Underline, Highlight

Formatted: Underline, Highlight

Formatted: Underline, Highlight

Formatted: Underline, Highlight

Formatted: Underline, Highlight

Formatted: Underline, Highlight

Formatted: Underline

Formatted: Underline, Highlight

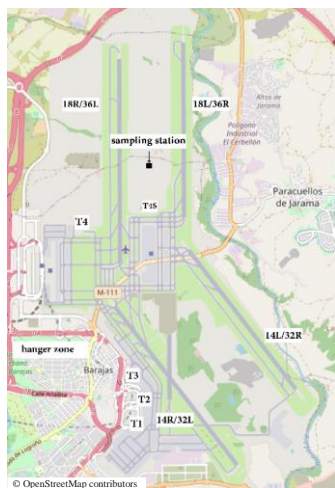


Figure 1. Locations of runways, terminals, and sampling site at Adolfo Suárez Madrid-Barajas Airport. Measurements were performed between October 8, 2021 and October 23, 2021. (Adapted from: <https://www.openstreetmap.org>)

119
120
121
122
123
124
125
126

2.2. Sampling and instrumentation

127
128 The autumn campaign of AVIATOR took place in October 2021. Sampling was conducted continuously, starting
129 at 12:00 pm on October 8, 2021 and ending at 20:00 pm on October 23, 2021. An ambient instrumentation system
130 with specific reference to PM was deployed at Madrid Airport to better characterise air quality at the airport
131 microenvironment. The measurement equipment of the system includes an Aerodyne High-Resolution Time-of-
132 Flight Aerosol Mass Spectrometer (AMS) for the chemical speciation of the particles. AMS measures
133 concentration and chemical composition of non-refractory aerosols online. AMS provided high-resolution
134 measurements of primary and secondary organic aerosol and inorganic aerosol including sulphates, nitrates, and
135 ammonium, from approximately 60 nm to 600 nm with 100 % transmission, extending to smaller and larger sizes
136 with reduced transmission (Canagaratna et al., 2007). An aerodynamic lens is used to draw aerosols into a vacuum
137 chamber. Particles are focused into a narrow beam and accelerated to a velocity inversely related to their vacuum
138 aerodynamic diameter. The particles impact on a tungsten surface, heated to 600 °C, which causes them to flash
139 vaporise. A 70-eV electron is used to ionize the vapours before they are analysed by mass spectrometry. During
140 the measurement period, AMS was sampling with 1µm cut-off inlet and at 30 s time resolution. In addition to
141 standard AMS flow, baseline and single ion calibrations every second day, an ammonium nitrate solution was
142 atomised to calibrate the AMS (for size-dependent ionisation efficiency). The analysis of the chemical
143 characteristics of aircraft PM using an AMS have been described elsewhere in detail (Yu et al., 2010; Anderson
144 et al., 2011; Smith et al., 2022). Equivalent black carbon mass concentration (*e*BC) based on aerosol optical
145 absorption was monitored using the Multi-Angle Absorption Photometer (MAAP) during this campaign. The
146 MAAP operates at 670nm wavelength, has a 10s-time response with a flow rate of 8 litre/min, for unattended
147 long-term monitoring of carbonaceous particulate emissions from combustion sources (Petzold and Schonlinner,
148 2004). MAAP has been used for the monitoring of black carbon emission from aviation (Herndon et al., 2008;
149 Timko et al., 2014). The instrument was set up to measure average *e*BC concentrations with one-minute intervals.
150 By using a condensation particle counter (CPC), TSI model 3750 ($D_{50} \approx 7\text{nm}$), total particle number concentration
151 was measured real-time to capture temporal variability in particle number concentrations with a measurement
152 range of up to 100,000 particles/cm³ and a time resolution of one second. Ambient CO₂ concentration near
153 runways were also measured by a LI-COR CO₂ Trace Gas Analysers at 1-sec intervals. In addition, meteorological
154 parameters (temperature, pressure, relative humidity, wind speed, and direction) were measured at the site with
155 the instrumentation system. The system was co-located with AENA (REDAIR) fixed monitoring site to provide
156 additional spatially resolved data. The REDAIR station monitors the concentration of sulphur dioxide (SO₂),

157 nitrogen dioxide (NO_x), carbon monoxide (CO), ozone (O₃), suspended particles PM (including PM_{2.5}, PM₁₀),
158 and total hydrocarbon (THC) with a time resolution of 30 minutes.

160 2.3. Data analysis

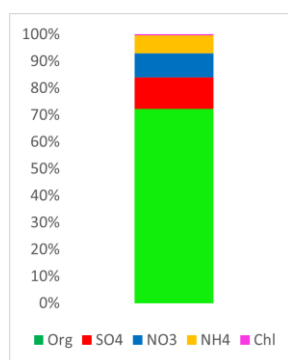
161
162 AMS was operating in Mass Spectrum (MS) mode to identify the chemical species present in the aerosol ensemble
163 and quantify the overall mass loading. AMS data were analysed using the data analysis toolkit TOF-AMS
164 SQUIRREL v1.65B, operated within Igor Pro (WaveMetrics, Inc.). The Source Finder (SoFi) is a software
165 package designed to analyse multivariate data using state-of-the-art source apportionment techniques to
166 understand the sources of various pollutants (Canonaco et al., 2013). SoFi, running under IGOR 6.37, was used
167 to deconvolve organic aerosol emissions via the Positive Matrix Factorization (PMF) model. The PMF model,
168 implemented through the multilinear engine version 2 (ME-2) factorisation tool, was used to determine the number
169 of factors (sources). ME-2, a multivariate solver, employs the same mathematical/statistical method as PMF to
170 evaluate solutions (Paatero, 1999). ME-2 equations are designed for analysing and calculating the relative
171 contributions of various source pollutants by measuring their concentration at receptor locations (Paatero and
172 Tapper, 1994). The PMF model processes many variables and categorises them into two types (i) source types,
173 which can be determined based on the chemical composition of the pollutants, and (ii) source contributions, used
174 to quantify the amount of contribution from each source to a sample. PMF inputs were restricted to only non-
175 negative concentrations since no sample can have a negative source contribution. A step-by-step approach was
176 employed to select the number of solutions (factors). The method described by Reyes et al. (2016) and Smith et
177 al. (2022) was followed, used to determine the optimal solution. This approach began initially with a two-factor
178 model and then incrementally increased to a maximum of five factors. PMF analysis was performed with seed
179 runs and varying FPEAK values (ranging from -1 to 1 with steps of 0.1) to better differentiate organic aerosol
180 sources. Seed runs and FPEAK are rotational techniques in the ME-2 tool, and they represent one of the
181 unconstrained PMF run approaches used for the exploration of the solution space. During the analysis, it was
182 noted that factor four consistently correlates with factor five, exhibiting identical time series and similarities in
183 mass spectra. This difficulty in separation has previously been observed in the case of well-mixed pollutants,
184 attributed to low temperatures and wind speeds (Reyes et al., 2018). Greater stability was achieved when analysing
185 3-factor solutions with varying FPEAK values. During the analysis, seed runs and PMF with FPEAK solutions
186 showed no significant variation in the normalised scaled residuals parameter (Q / Q_{exp}), with values close to 1.
187 This is reasonable given that PMF determines the solution by minimising this value (Reyes et al., 2016). The
188 factorisation strategy was entirely successful in separating three different sources, each with distinct mass spectra
189 and differing time series. Consequently, 3-factor solutions emerged as the optimal number of sources,
190 demonstrating the best performance with the lowest residuals and Q/Q_{exp} values close to 1. Furthermore, the
191 obtained solution exhibited the most favorable results, characterized by distinct diurnal trends and dissimilarities
192 in time series and mass-to-charge ratios among the factors.

Formatted: Underline, Highlight

195 3. Results and Discussion

196 3.1 Variations of organic, inorganic, and oil emissions

197



198
199
200
201
202

Figure 2. The bar chart shows aerosol fractions where organic and sulphate species account for more than 80% of the total aerosol mass.

203 Mass concentrations of organic and inorganic aerosols was $9.6 \mu\text{g}/\text{m}^3$ on average for the entire campaign. Organic
 204 aerosols, with a significantly high fraction compared to the nearest sulphate with 15 % accounts for about 70% of
 205 the total aerosols measured by AMS. Figure 2 shows aerosol fractions where organics account for about 70% of
 206 the aerosol. The average mass concentration of organic and inorganic aerosols during the entire campaign was 9.6
 207 $\mu\text{g}/\text{m}^3$. The bar chart in Fig. 2 shows aerosol fractions, with organic species accounting for more than 70% of the
 208 total aerosols. This is significantly higher than the nearest component, sulphate, which accounted for 15%. It
 209 should also be noted that the nitrate and sulphate species measured by AMS could potentially contain an organic
 210 fraction. The PMF analysis in this paper mainly focuses on the composition of the organic mass concentration.
 211 The PMF analysis in this paper primarily focuses on the composition of the organic mass concentration, which is
 212 discussed in further detail in Section 3.2. Previous studies have shown that lubrication oil has been detected in
 213 ambient air near runways, and it may further add to the total organic PM emissions due to aircraft engine
 214 operations (Timko et al., 2010b; Yu et al., 2010; Fushimi et al., 2019; Ungeheuer et al., 2022). Aircraft plume
 215 measurements indicated that oil was found to contribute 5% to 100% (Yu et al., 2012). The m/z 85 signal is a
 216 well-known oil signal in the AMS mass spectrum. The m/z 85 signal is a well-known oil marker in the AMS mass
 217 spectrum, attributed to synthetic esters ($\text{C}_5\text{H}_8\text{O}^+$) (Timko et al., 2014). Ratio of m/z 85:71 is used as a marker for
 218 oil (Fig. 3). The value of 0.66 was used as a benchmark for oil contribution (Yu et al., 2012). A value less than
 219 0.66 can be considered oil-free organic PM and conversely, any value larger than 0.66 indicates the presence of
 220 lubrication oil. Values below 0.66 indicate oil-free organic PM, while values above 0.66 suggest the presence of
 221 lubrication oil. However, based on the AMS measurements during AVIATOR autumn campaign, lubrication oil
 222 accounted only up to 5% of the total aerosol mass, which is significantly less compared to the measurements of
 223 Yu et al. (2012). There are three probable explanations on the deficiency of AMS to detect oil precursors: (i) the
 224 oil particles are too small in diameter for AMS to detect, (ii) complete pyrolysis of the oil in the engine combustion
 225 zone forming carbon monoxide (CO) and carbon dioxide (CO_2) (Smith et al., 2022) or (iii) oil particles contribute
 226 to an insignificant amount (by mass) of to the organic mass in engine exhaust and therefore are not detected.
 227 Additional factors that could potentially impact the minimal presence of oil lubrication in this analysis might
 228 involve the overall mass loading of aerosols, the influence of urban aerosol emissions, or the proximity of the
 229 sampling point to the nearest runways. Additional information on how the lubrication oil ratio, as measured by
 230 AMS, varies with wind speed and direction is provided in the supplementary material (Fig.S4). During the
 231 AVIATOR autumn campaign, measuring oil was challenging due to the prevalent urban background. A "little oil"
 232 region was identified at low to moderate wind speeds (2~5 m/s) originating from the southwest, encompassing
 233 terminal buildings (T1, T2, T3, T4, and TS4), two runways (14R/32L and 18R/36L), and a hangar zone. In
 234 contrast, a region "unlikely to contain oil" was noted when winds came from the northeast of the airport, near
 235 runways 18L/36R, with relatively higher wind speeds (above 5 m/s). Furthermore, Fig.S5 displays the daily
 236 lubrication oil ratio of m/z 85:71 throughout the sampling period, pinpointing Sunday, October 16th, as the only
 237 day when the lubrication oil marker surpassed 0.66. On other days, the ratio of m/z 85:71 suggested a minimal
 238 likelihood of oil presence. An hourly analysis within Fig.S5 reveals that the lubrication oil marker exceeded 0.66
 239 only at 20:00, aligning with the evening peak in $\text{PM}_{2.5}$ concentrations Fig.S3. This suggests a significant influence
 240 of urban background aerosols on the lubrication oil measurements. Since PMF analysis is based on the organic
 241 masses measured via AMS, lubrication oil is not identified as a determinant and there is no oil organic mass profile
 242 reported in previous studies and here (Ulbrich et al., 2009). PMF has been proven inefficient at detecting such
 243 levels (Ulbrich et al., 2009), therefore, oil contribution to the organic mass may be under-represented in this study.

Formatted: Underline, Highlight

Formatted: Underline, Highlight

Formatted: Underline, Highlight

Formatted: Underline, Highlight

Formatted: Underline, Highlight

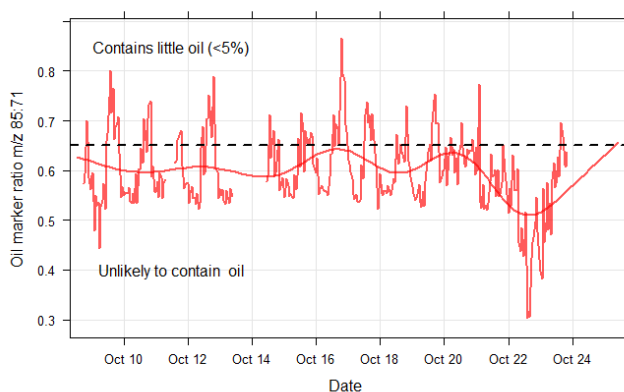
Formatted: Underline, Highlight

Formatted: Underline, Highlight

Formatted: Underline, Highlight

Formatted: Underline, Highlight

Formatted: Underline, Highlight



244

245 **Figure 3. Temporal variability of lubrication oil fraction in total aerosol mass obtained from AMS measurements.**
 246 **The ratio of m/z 85/71 was used as the mass marker to identify lubrication oil. A smooth red line is fitted to the data,**
 247 **while the dashed black line represents the value of 0.66, assumed for oil-free organic PM emitted from aircraft**
 248 **engines. The analysis showed that no oil or very little (<5%) oil fraction was detected during the measurement period.**

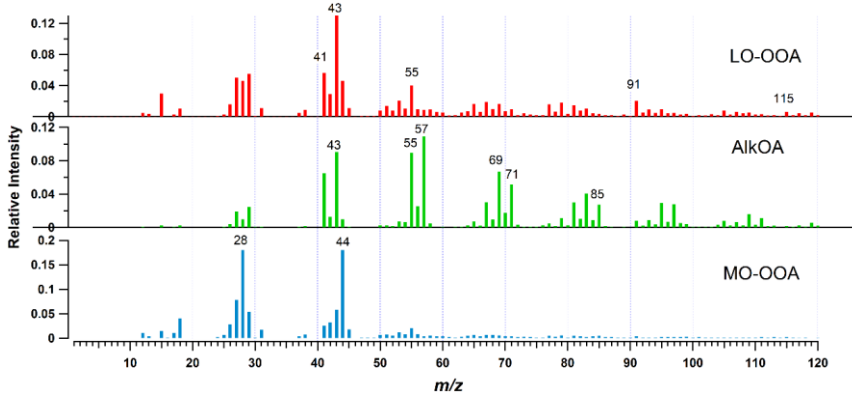
Formatted: Underline, Highlight

3.2 PMF Analysis

249

250

251



252

253

254

255

256

257

258

259

260

261

262

263

264

265

266

267

268

269

270

271

272

273

274

275

276

277

278

279

280

281

282

283

284

285

286

287

288

289

Figure 4. The mass spectral fingerprint of the three factors from the PMF solutions. Less Oxidised Oxygenated Organic Aerosol (LO-OOA), Alkane Organic Aerosol (AlkOA), and More Oxidised Oxygenated Organic Aerosol (MO-OOA), which can be indicative of secondary aerosols. Selected mass markers with a relative intensity higher than 0.01 are numbered.

The PMF analysis in this study aims to provide relative contribution of the sources of aerosols near runway. In addition to determining the diurnal pattern of the obtained factors during the autumn campaign, PMF solutions were used to investigate how meteorology affects airborne particulate pollution. During AVIATOR autumn campaign at Madrid-Barajas International Airport three sources were identified via PMF (Fig. 4 shows the results of the PMF analysis, the mass spectral fingerprint). The first factor in Fig. 4, LO-OOA, stands for Less Oxidised Oxygenated Organic Aerosol. It is a type of secondary organic aerosol (SOA) characterized by its low degree of oxidation. LO-OOA are formed in the atmosphere through the oxidation of volatile organic compounds (VOCs), which can originate from a variety of anthropogenic sources. In this analysis LO-OOA shows the presence of an aromatic marker at m/z 115, a marker used for identifying indene (C_9H_8) ion in previous studies focusing on aviation emissions (Timko et al., 2014; Smith et al., 2022). LO-OOA is associated with aromatic fragments at m/z 77, 91, 105, 115 and presents a high relative intensity (0.13) at m/z 43 (characteristic of LO-OOA) and a lower relative intensity (<0.04) at m/z 91 which is related to toluene ion ($C_7H_7^+$) (Smith et al., 2022). LO-OOA is associated with aromatic fragments at m/z 77 ($C_6H_5^+$), and 105 ($C_8H_9^+$). It presents a high relative intensity (0.13) at m/z 43 ($C_3H_7^+$) (characteristic of LO-OOA) and a lower relative intensity (<0.04) at m/z 91, which is related to toluene ion ($C_7H_7^+$) (Timko et al., 2014; Smith et al., 2022). Ambient temperature plays a crucial role in influencing the LO-OOA factor, displaying significant diurnal fluctuations. The lowest concentrations of LO-OOA are recorded at midday, coinciding with the peak in ambient temperatures (Fig. 5). A prior PMF analysis of organic particulate matter from aircraft emissions revealed a significant aromatic factor within the organic PM, characterized by elevated signals at m/z 77, 91, 105, 115, 128 (Timko et al., 2014). The aromatic factor identified by Timko et al. (2014) was found to dominate the organic PM emissions from turbojet engines at low-thrust settings. It was associated with the products of incomplete combustion and exhibited high variability, which varied with engine power settings (the sum of signals in the factor decreased as engine power increased). Another study by Smith et al. (2022), investigated the chemical composition of organic aerosols emitted by gas turbines and identified a Semi-Volatile Oxygenated Organic Aerosol (SV-OOA) factor, which forms through oxidative processes near the engine exit. A strong correlation ($R = 0.91$) and similarity in mass spectra between the LO-OOA in this study and the SV-OOA described by Smith et al. (2022) were observed. Owing to the absence of volatility measurements during this period and the limited time for aging (no more than a few minutes), we consider the LO-OOA factor in our analysis to be the most accurate estimate available, rather than the SV-OOA as suggested by Smith et al. (2022). The second factor, identified based on the PMF analysis of Madrid airport sample, is Alkane Organic Aerosol (AlkOA) factor. It is associated with unburned fuel and emissions from

Formatted: Underline, Highlight

Formatted: Underline, Highlight

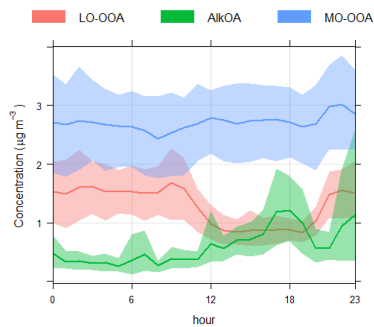
Formatted: Underline, Highlight

Formatted: Underline, Highlight

Formatted: Underline, Highlight

290 incomplete combustion, exhibiting high relative intensities at m/z 43, 57, and 85, indicative of decane ($C_{10}H_{22}$), a
 291 common alkane in jet fuel. Given that mass spectral fingerprint of decane is similar to the other aliphatic
 292 hydrocarbons (*e.g.*, long-chain alkanes) found in Jet A1 fuel, as reported by Yu et al. (2012) and Smith et al.
 293 (2022). AlkOA factor referred here as a marker to identify emissions originating from unburnt fuel/incomplete
 294 fuel combustion products. Previously, primary aliphatic factor was found in PMF analysis by Timko et al. (2014)
 295 and was characterized by increased signals at masses such as 41/43, 55/57, 69/71, 83/85. Each of these masses
 296 correspond to an alkane. The primary aliphatic factor in Timko et al. (2014) study was strongly correlated with
 297 black carbon soot emissions under high-power conditions. The strong association between the primary aliphatic
 298 factor and soot emissions suggests they originate from similar combustion processes. Timko et al. (2014)
 299 concluded that the primary aliphatic factor is derived from combustion related sources and can potentially contain
 300 significant amounts of unburnt jet fuel. Additionally, a strong positive linear correlation was observed between
 301 the AlkOA factor identified in this study and the decane factor from NIST webbook ($R=0.83$) (NIST Mass
 302 Spectrometry Data Center, 1990), as well as between the AlkOA factor determined here and the AlkOA factor
 303 reported by Smith et al. (2022) ($R=0.93$). The positive linear correlation among these three factors suggests they
 304 are indicative of similar primary pollutants derived from fuel vapours or incomplete combustion products
 305 associated with jet fuel. Results are consistent with previous findings of another study (Smith et al., 2022). The
 306 third factor, More Oxidised Oxygenated Organic Aerosol (MO-OOA), is a type of secondary organic aerosol
 307 (SOA) that can form from various origins and processes, such as photochemical processing of aged SOA and the
 308 regional-scale transport of chemical reactions. MO-OOA has a spectral fingerprint that consists of more oxidised
 309 ions (compared to LO-OOA and AlkOA), indicating a secondary aerosol fraction in the sample. MO-OOA is
 310 characterized by its notably high relative intensities (>0.18) at m/z 29 and 44, which serve as markers for its
 311 identification. MO-OOA is characterized by its notably high relative intensities (>0.18) at m/z 29 (CHO^+) and 44
 312 (CO_2^+), which serve as markers for its identification (Alfarra et al., 2007). Given that MO-OOA has the highest
 313 $f_{44/43}$ ratio among the three factors, it is expected to be the most oxygenated (in terms of chemical content) factor.
 314 Being more oxidised potentially makes MO-OOA less volatile than LO-OOA (Jimenez et al., 2009; Smith et al.,
 315 2022). MO-OOA in this analysis indicates the formation of aged secondary organic aerosols with no significant
 316 diurnal variation (Fig. 5), often associated with air masses transported from polluted regions. Other sources may
 317 have been included in one or both factor solutions, consequently, this does not rule out the possibility of their
 318 existence.

3.3 The temporal distribution of factors and correlation with trace gases



323 Figure 5. Diurnal pattern of the solved factors from October 8, 2021 to October 23, 2021. The mean diurnal pattern is
 324 shown as solid lines, and the shading indicates the 95% confidence interval around the mean.
 325

326 Average hourly concentrations of the PMF-determined factors were calculated based on the hourly organic aerosol
 327 concentrations throughout the entire campaign to monitor the diurnal variation of the source contributions. The
 328 variation of the AlkOA concentration during the day mostly associated with aircraft emissions (Fig. 5). The
 329 concentration of AlkOA factor is relatively higher in the afternoon compared to the morning and midday. The
 330 pattern of diurnal AlkOA closely resembles that of diurnal flight activities, suggesting that the surge in AlkOA
 331 levels beginning at noon is linked to primary particles released by aircraft. The AlkOA factor shows an increase
 332 between 09:00 and 20:00 and again between 22:00 and 23:00. Based on the mean diurnal pattern with a 95%
 333 confidence interval, the AlkOA factor increases during the 09:00 to 20:00 period, corresponding with peak flight
 334 activity (approximately 71% of total flights). Further details on daily aircraft activities are provided in the
 335

Formatted: Underline, Highlight

Formatted: Underline, Highlight

Formatted: Underline, Highlight

Formatted: Underline, Highlight

Formatted: Underline, Highlight

Formatted: Underline, Highlight

336 supplementary material (Fig. S2). The increase in AlkOA between 22:00 and 23:00 is not statistically significant
337 due to high variability (Fig. 5). The increase in AlkOA concentration from 22:00 to 23:00, or the subsequent
338 decrease from 23:00 to 00:00, falls within the variability range of the 00:00 to 01:00 period. Therefore, a
339 statistically significant decrease in AlkOA concentration from 23:00 to 00:00 is hardly measurable.
340 Meteorological factors may contribute to the variability in the diurnal cycle observed during this period.
341 Additionally, unidentified local source such as airport ground service equipment could potentially explain the
342 variability observed from 22:00 to 00:00. This source has been previously reported as the main determinant of the
343 air quality in the vicinity of the airport (Masiol and Harrison, 2014). The LO-OOA factor likely represents fresh
344 secondary organic aerosols (SOA), demonstrating high variability and sensitivity to ambient temperature
345 fluctuations. The concentration of LO-OOA is at its lowest when daytime temperatures peak. LO-OOA may
346 contain urban contributions and potentially effected by background urban pollution from Madrid. The observed
347 reduction in LO-OOA factor during the afternoon can be attributed to dilution effects resulting from the rise in
348 boundary layer height, along with the potential evaporation of LO-OOA particles due to increased ambient
349 temperatures. This is supported by the variance in background particulate matter concentrations located south of
350 the airport compared to those at the sampling point, approximately 6 km apart, as illustrated in Fig. S3. (Fig. S3)
351 reveals that PM_{2.5} levels at both locations experience significant increases during morning and evening rush hours,
352 with the sampling point consistently showing higher concentrations than the background location. The diurnal
353 pattern of the background location demonstrates a rapid decrease in PM_{2.5} levels in the afternoon, unlike the
354 measurements at the sampling point. Additionally, there is a noticeable lag of about an hour between the peak
355 concentrations at the sampling point and those in the background, suggesting the influence of additional
356 combustion sources of PM_{2.5}, notably aviation-related activities, particularly during periods of increased airport
357 traffic. Unlike other factors, MO-OOA shows no significant diurnal variation, indicating the formation of aged
358 secondary organic aerosols, often a result of atmospheric transport (Zhang et al., 2007). Detailed statistics of the
359 obtained factors for the entire campaign are provided in the supplementary material (Table S1). At Madrid-Barajas
360 Airport, AlkOA exhibited moderate correlations with eBC, NO_x, SO₂, and CO, as evidenced by the linear
361 correlation coefficients listed in Table 1 (R=0.56, R =0.52, R =0.53, and R =0.52). In contrast, the correlation of
362 these trace gases and both LO-OOA and MO-OOA is lower compared to AlkOA, with R values ranging from 0.2
363 to 0.5, as shown in (Table 1). The slightly higher correlation of AlkOA with BC, NO_x, SO₂ and CO (R > 0.5)
364 relative to LO-OOA and MO-OOA can be attributed to AlkOA being a primary pollutant, emitted directly from
365 the source. Conversely, LO-OOA and MO-OOA are believed to be secondary pollutants, formed through the
366 processes of condensation and coagulation of primary pollutants. In this study, urban contributions are
367 predominantly subject to this processing, as there is insufficient time for significant photochemical oxidation of
368 aviation emissions in such close proximity to the source. Additionally, the diurnal trends of BC, NO_x, SO₂ and
369 CO can be significantly affected by meteorological conditions (e.g., wind speed, temperature) (Carslaw et al.,
370 2006; Reyes et al., 2018). This influence accounts for their moderate correlation with AlkOA, with R values
371 between 0.52 and 0.56, as detailed in Table 1. Similarly, AlkOA could potentially be affected by meteorological
372 conditions. Since AlkOA is measured as part of AMS sub-micron particles, it is expected to behave similarly to
373 eBC in the particle phase. Therefore, meteorological conditions likely influence both AlkOA and eBC in a similar
374 manner. AlkOA and trace gases were normalised to facilitate comparison of their diurnal patterns, thereby
375 enhancing understanding of their relative contributions and identifying trends among these pollutants.
376 Normalising is accomplished by dividing the concentrations of the pollutants by their average value. Figure 6
377 shows diurnal patterns of AlkOA factor, eBC, NO_x, CO, and particle number concentration. The daily trend of
378 eBC, NO_x and CO are mostly similar, with very pronounced increases in concentrations during the morning and
379 evening rush hours. The average concentrations were 1.07 µg/m³, 22.7 µg/m³ and 0.23 mg/m³ for eBC, NO_x and
380 CO respectively (Table S1). AlkOA gradually increases during the morning, with multiple minor peaks observed
381 in the morning hours. The average concentration of AlkOA is higher at night than during the day. This increase
382 is potentially related to daily aircraft activities. AlkOA began to increase, reaching a maximum during the
383 afternoon rush hour from 12:00-18:00. A second rapid increase occurred around 20:00, potentially caused by an
384 increase in the number of flights at this time (Fig. S2). Early morning AlkOA concentrations are significantly
385 lower compared to those of eBC, NO_x, and CO. This difference could be attributed to reduced emissions resulting
386 from decreased aircraft activities in early mornings (Fig. S2). The rise in trace gases and eBC observed in the
387 early morning hours could originate from various airport operations. Such operations might encompass emissions
388 from auxiliary power units, vehicle traffic, and the use of ground service equipment at the airport (Masiol and
389 Harrison, 2014). The total number concentration exhibited a temporal pattern similar to that of AlkOA from
390 15:00–21:00. Likewise, the temporal profiles of AlkOA and trace gases were similar during the afternoon period
391 (17:00–21:00). This similarity in temporal profiles suggests common source origins, which may be temporally
392 associated with aircraft activity or the influence of background urban pollution.

393
394 **Table 1 Results of linear regression analysis between obtained factors (LO-OOA, AlkOA, and MO-OOA)**
395 **and external tracers. Data from the entire campaign was used to perform the correlation analysis.**

Formatted: Underline, Highlight

Formatted: Underline, Highlight

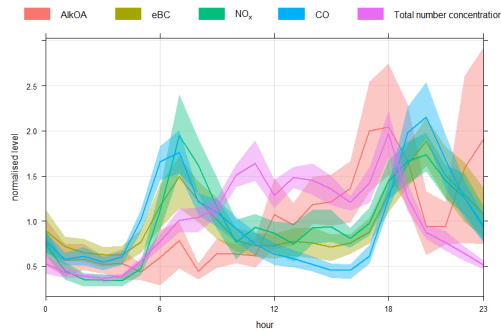
Formatted: Underline, Highlight

Formatted: Underline, Highlight

396

| | eBC ($\mu\text{g}/\text{m}^3$) | NO _x ($\mu\text{g}/\text{m}^3$) | SO ₂ ($\mu\text{g}/\text{m}^3$) | CO (mg/m^3) | THC (mg/m^3) | PM _{2.5} ($\mu\text{g}/\text{m}^3$) | Tot No. conc (particles/cm ³) | CO ₂ (ppm) |
|--------|-------------------------------------|---|---|----------------------------------|-----------------------------------|---|--|--------------------------|
| LO-OOA | 0.49 | 0.28 | 0.21 | 0.32 | 0.63 | 0.36 | -0.08 | 0.24 |
| AlkOA | 0.56 | 0.52 | 0.53 | 0.52 | 0.35 | 0.66 | 0.4 | 0.35 |
| MO-OOA | 0.48 | 0.36 | 0.26 | 0.45 | 0.41 | 0.55 | 0.1 | 0.22 |

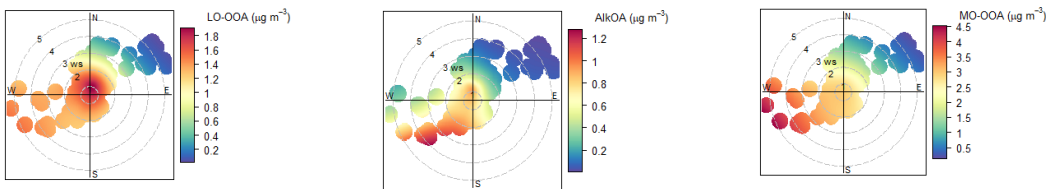
397
398
399
400



401
402
403
404
405
406
407

Figure 6. The diurnal cycle of AlkOA compared to eBC, NO_x, CO, and total number concentration. In this plot, the concentrations are normalised with the objective of comparing the patterns of different pollutants using the same scale.

3.4 Spatial analysis

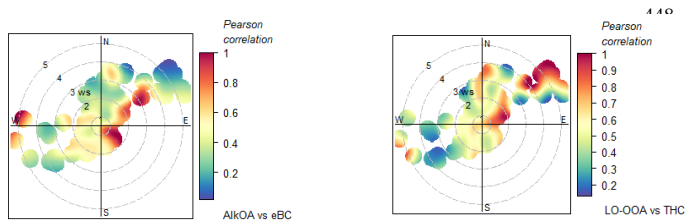


408
409
410
411
412
413
414
415
416
417
418
419
420
421
422
423
424
425

Figure 7. Bivariate polar plots for LO-OOA, AlkOA, and MO-OOA ($\mu\text{g}/\text{m}^3$). The highest concentrations were measured when the winds were originated from the west and southwest. Runways 18R/36L and 14R/32L located at western and eastern sides of the measurement station and the hanger zone with terminals T1, T2, T3, T4, and TS4 are located at the south and southwest of the measurement site (Fig. 1).

Varying sources can be discriminated by means of bivariate polar plots techniques (Carslaw and Ropkins, 2012). Figure 7 illustrates the impact of airport activities on the average concentrations of factors (LO-OOA, AlkOA and MO-OOA) as determined by PMF. The highest concentrations of AlkOA and MO-OOA were observed at low to moderate wind speeds (3–5 m/s) coming from the west and southwest ($R = -0.35$ and $R = -0.42$, respectively), near the terminal buildings (T1, T2, T3, T4 and TS4), two of the runways (14R/32L and 18R/36L), and a nearby hanger zone. The most significant contributions of LO-OOA occur at wind speeds below 2 m/s, with a correlation of $R = -0.45$. At such low wind speeds (< 2 m/s), LO-OOA and MO-OOA are more likely to be mixed and influenced by a nearby source (Crilley et al., 2015; Helin et al., 2018). By contrast, the minimum significant contribution from all factors was observed when the winds originated from the northeast of the airport, accompanied by relatively higher wind speeds (above 4 m/s). Thus, based on the polar plots shown in Fig. 7, emissions from the terminal buildings and hanger zone located at the southwest of the measurement station are the major sources of total organic particle concentrations at the measurement station. The average contributions of LO-OOA, AlkOA,

426 and MO-OOA were 1.63, 0.63, and 2.35 $\mu\text{g}/\text{m}^3$, respectively (Table S1). During the AVIATOR campaign in
 427 October 2021, LO-OOA and MO-OOA constituted more than 80% of the total organic mass. Based on the strength
 428 of the relationship outlined in Table 1 between derived factors and external tracers, the linear correlations (Pearson
 429 correlation) between (i) AlkOA with *e*BC and (ii) LO-OOA with THC were measured under varying wind speed
 430 and directions, as illustrated in (Fig. 8). The relative contributions of the AlkOA and LO-OOA were higher with
 431 winds originating from southwest of the airport, compared to when winds carried air parcels to the sampling point
 432 from the northeast, as discussed. However, the correlation coefficient for these factors varies significantly, ranging
 433 from 0.2 to 0.9, for all samples collected from various directions within the airport perimeter. For instance, AlkOA
 434 exhibits a strong linear correlation with *e*BC (Pearson coefficient higher than 0.9) when winds originate from the
 435 west, east, or northeast, as illustrated in Fig. 8. This correlation is attributed to the impact of runways 18L/36R
 436 and 18R/36L, which are situated to the east and west of the measurement site, respectively, as depicted in Fig. 1,
 437 where 90% of aircraft take-offs occur. Both AlkOA and *e*BC are related to jet fuel emissions, as they are directly
 438 emitted by aircraft engines as a result of fuel combustion. *e*BC emissions are a function of engine power settings,
 439 reaching their maximum at full thrust during take-off (Kinsey et al. 2011; Hu et al., 2009). Furthermore, a
 440 significant linear correlation was measured between LO-OOA and THC when dominant winds were north
 441 easterlies (the air parcels move from runways 18L/36R to the sampling station). THC emissions at airports
 442 primarily dependent on the jet engine thrust setting (Anderson et al., 2006; Onasch et al., 2009). When engines
 443 operate at low thrust settings (*e.g.*, during landing, taxiing, idling), combustion is less efficient, leading to the
 444 emission of higher amounts of hydrocarbons. The association between LO-OOA and THC in certain areas of the
 445 airport can be interpreted as indicative of fresh emissions from aircraft in service.
 446
 447

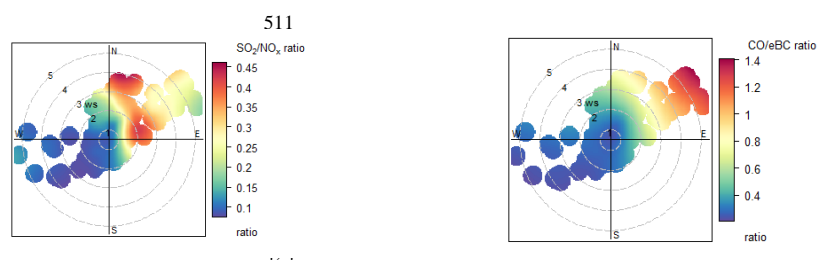


461
 462 **Figure 8. A Pearson correlation analysis using bivariate polar plots (above) shows a significant positive linear**
 463 **correlation between AlkOA with *e*BC and LO-OOA with THC mass concentrations when prevailing winds were**
 464 **northeast. (The location of runways 18L/36R).**
 465

466 NO_x emitted by aircraft can potentially affect air quality up to 2.6 km away from the airport (Carslaw et al., 2006).
 467 However, accurately determining the airport's contribution to local NO_x concentrations presents challenges due
 468 to other predominantly mobile sources of NO_x in urban areas. In this study, the potential contribution of road
 469 traffic surrounding the airport, particularly from the motorways located to the south and southwest, originates
 470 from the same direction as runway 14R/32L and all the terminals. Therefore, NO_x contributions were higher from
 471 the south and southwest of the airport (including local on-road NO_x) compared to the those from the northeast.
 472 The lowest NO_x concentrations were measured under moderate wind speed conditions (above 4 m/s), as shown in
 473 Fig. S1. This is possibly due to atmospheric mixing and plume dilution caused by advection (Carslaw et al., 2006),
 474 given that ground-level source emissions are inversely proportional to wind speed. During this campaign, the
 475 AENA (REDAIR) station located at the airport provided measurements of sulphur dioxide (SO_2) and carbon
 476 monoxide (CO) (Fig. S1). Aviation activities have previously been reported as a significant source of gaseous and
 477 vapour-phase pollutants, such as SO_2 , CO and NO_x (Masiol and Harrison, 2014). In the same vein, mobile sources,
 478 such as vehicle exhaust, generally contribute to the increase in CO and NO_x levels, as motor vehicle emissions
 479 are the dominant sources of CO and NO_x emissions in urban areas (Yu et al., 2004). Given that Barajas airport is
 480 situated near Madrid and significantly influenced by external sources, particularly traffic on the southwest side of
 481 the airport, it experiences considerable environmental impact. Therefore, the ratios of SO_2/NO_x and $\text{CO}/e\text{BC}$ were
 482 used in this analysis as indicators of the relative emission strengths associated with aircraft movements. The
 483 SO_2/NO_x ratio would increase in the case of aviation emissions compared to traffic emissions, since NO_x emissions
 484 from aircraft are difficult to distinguish due to the major influence of other sources (Yu et al., 2004; Carslaw et
 485 al., 2006). Consequently, in situations where there are substantial levels of NO_x emissions, the SO_2/NO_x ratio will
 486 be low due to the impact of on-road vehicles emissions. This enables the identification of aircraft's relative
 487 contribution at the airport, as shown in Fig.9. The analysis of the SO_2/NO_x and $\text{CO}/e\text{BC}$ concentration ratios at

488 Madrid-Barajas Airport in October 2021 varies based on wind direction and speed. The bivariate polar plots shown
 489 in Fig. 9 indicate higher SO_2/NO_x and $\text{CO}/e\text{BC}$ ratios were measured when dominant winds originating from the
 490 northeast of the airport, where there was minimal or no contribution from road traffic. The higher SO_2/NO_x and
 491 $\text{CO}/e\text{BC}$ ratios suggest the potential impact of aircraft taxiing and taking off on local ambient SO_2 and CO
 492 concentrations, particularly when winds originate from northeast, where the 18L/36R runways are located. SO_2
 493 emissions are primarily associated with the sulphur content of the fuel and emissions from aircraft activities at the
 494 airport, such as approach, taxi-idle and climb. As a result, SO_2 plays a significant role in tracing aircraft emissions
 495 at a local scale (Yang et al., 2018). Black carbon ($e\text{BC}$) and carbon monoxide (CO) are primarily produced by
 496 incomplete or inefficient combustion. Around the airport perimeter, aircraft are a significant contributor to CO
 497 emissions. Therefore, it's possible for aircraft engines to emit more CO compared to emissions from road traffic,
 498 due to the duration spent at the airport in taxiing /idling mode (Yu et al., 2004; Zhu et al., 2011). The $\text{CO}/e\text{BC}$
 499 ratio significantly varies with the source (Bond et al., 2004), indicating the presence of different emission sources
 500 in the vicinity of the airport, as previously reported. The highest levels of CO from aircraft are emitted at low
 501 engine power settings, such as during taxiing and idling. This significantly impacts air quality within the airport
 502 perimeter, as idle and taxi phases constitute the majority of the time an aircraft spends at the airport (Stettler et
 503 al., 2011; Yunos et al., 2017). Higher $\text{CO}/e\text{BC}$ ratio in air parcels originating from the northeast can also be
 504 attributed to aircraft activity on runways 18L/36R, which is located northeast of the measurement station.
 505 Conversely, SO_2/NO_x and $\text{CO}/e\text{BC}$ ratios were lower (ranging from 0 to 0.4) when winds originated from the
 506 southwest, due to significant sources of NO_x and $e\text{BC}$ in this direction, such as nearby road traffic. Based on the
 507 polar plots shown in Fig. 9, an aircraft SO_2 and CO signal is identified to the east and northeast, distinct from the
 508 wind-dependant NO_x pattern. Further details regarding the daily variation of meteorological parameters and trace
 509 gases during the sampling period are available in the supplementary material (Fig. S1).

510



526

527

528

529

Figure 9. Bivariate polar plots of SO_2/NO_x and $\text{CO}/e\text{BC}$ ratios at the airport. The angular contributions of SO_2 and CO is different compared to the PMF determined factors. The plots indicate that the flight activities at the east and northeast where the 18L/36R runway is located are the source of increase in SO_2 and CO .

530

531

532

4. Conclusion

533

534

535

536

537

538

539

540

541

542

543

544

545

546

547

548

549

550

This study identified the impact of an international airport on the local air quality. As part of the AVIATOR campaign, several measurements were conducted at the Madrid-Barajas Airport, in October 2021 for monitoring the chemical composition of sub-micron particles and ambient trace gas concentrations near runway. Assessing the impact of Madrid-Barajas Airport emissions on local air quality is challenging because of the complex nature of airport emissions and the strong influence from urban emissions. The proximity of the airport to urban areas, major highways, roads, and terminal buildings (T1, T2, T3, T4 and TS4) further complicates the task, making it difficult to clearly identify the specific contributions of aircraft emissions. However, aircraft emissions are characterized by high levels of unburned hydrocarbons, SO_2 , CO and particulate black carbon ($e\text{BC}$) which are more concentrated around the airport facilities and runways. Therefore, looking at elevated levels of these markers might indicate a stronger influence from aviation-related activities, especially during times of high airport traffic. Total non-refractory particles were dominated by organics (more than 72% of the total). Sulphate particles were the second most abundant chemical species and accounted for about 13% of the total aerosol. Based on AMS data (Ratio of m/z 85:71), no significant oil fraction in the organic particulate matter (PM) samples were measured. This could indicate the absence of oil in sub-micron particle size range or due to the method used in this study (AMS) is not able to identify lubricant oil in PM. Thus, further measurements with improved measurement technique may be required to identify oil fraction in sub-micron organic aerosol. Trace gases were also monitored along with the particle monitoring tools. Average ambient concentrations of $e\text{BC}$, NO_x , SO_2 , $\text{PM}_{2.5}$, PM_{10} at the airport during October 2021 were 1.07, 22.7, 4.10, 9.35, and 16.43 ($\mu\text{g}/\text{m}^3$), respectively. NO_x contribution at the

551 sampling point was highest when the winds originating from south and southeast of the airport. There are two
552 motorways with road traffic are located at the same direction as well as terminal buildings and southern runways.
553 Therefore, NO_x concentrations were more likely determined by on-road traffic compared to the aircraft activity at
554 the sampling point. Sources of organic aerosols (as the most abundant non-refractory aerosol group) were
555 identified using Positive Matrix Factorisation (PMF) analysis. PMF was able to discriminate three main significant
556 sources: Less Oxidised Oxygenated Organic Aerosol (LO-OOA), Alkane Organic Aerosol (AlkOA), and More
557 Oxidised Oxygenated Organic Aerosol (MO OOA). The sum of LO-OOA and MO OOA fractions accounting for
558 more than 80% of the total organic mass throughout the campaign, LO-OOA had the highest relative intensity
559 (RI) at *m/z* 43 (which is characteristic of LO-OOA), MO-OOA had a high RI at *m/z* 28 and 44 these indicate a
560 potential secondary aerosol fraction. Third factor, AlkOA, had high RIs at *m/z* 43, 57 and 85 (attributed to decane
561 previously) which is related to jet fuel vapour (Smith et al., 2022). Bivariate polar plots were used to angular PMF
562 determined factor and ambient trace gas distributions based on wind speed and wind direction at the airport. It has
563 been found that, the PMF determined factors had highest relative contributions when the winds originating from
564 the west and southwest of the airport where runways 14R/32L and 18R/36L, as well as terminals T1, T2, T3, T4
565 and TS4, are located. The SO₂/NO_x and CO/*e*BC ratio have been shown to represent a useful tool for assessing
566 relative emission strength associated with aircraft movements. Take-off activities at the northeast of the
567 measurement station were identified as a potential local source of SO₂ and CO in Barajas-Madrid. Angular
568 correlation analysis based on wind direction and speed indicated that *e*BC and THC emissions are potentially
569 determined by aircraft take off activities at 18L/36R runway located along the east and northeast of the sampling
570 point where more than 50% of the take-off activity took place in the sampling period.
571 There are two previously reported significant ways to reduce aviation emissions at airports, improving efficiency
572 of the processes emitting air pollutants such as electrification of airport taxiway operations (Salihu et al., 2021),
573 and switching to sustainable alternative fuels where applicable. Improved ground activities at airports such as
574 electric aircraft towing system can potentially lead up to 82 % reduction in CO₂ emissions (van Baaren, 2019),
575 while switching to SAF alone reduce Landing-takeoff cycle (LTO) emissions up to 70 % compared to fossil fuel
576 (Schripp et al., 2022). Further, SAF use for auxiliary power units (APU) also potentially reduce NO_x and CO₂
577 emissions by at least 5%. Therefore, improving energy efficiency of ground activities at airports and using SAF
578 are recommended for policymakers to improve the overall air quality at airports.

579
580 *Author contributions.* **Saleh Alzahrani, Doğuşhan Kılıç, Michael Flynn, Paul I. Williams and James Allan**
581 designed the project; **Saleh Alzahrani, Doğuşhan Kılıç, Michael Flynn and Paul I. Williams** performed the
582 fieldwork; **Saleh Alzahrani** performed the data analysis, and wrote – original draft of the article; **Doğuşhan**
583 **Kılıç** reviewed and edited the article; **Paul I. Williams and James Allan** supervised, reviewed and edited the
584 article.

585
586 *Competing interests.* At least one of the (co-) authors is a member of the editorial board of Atmospheric
587 Chemistry and Physics.

588 **Acknowledgments**

589
590
591 This project has received funding from the European Union's Horizon 2020 research and innovation programme
592 under Grant Agreement No 814801.

593 **References**

594
595
596 Air transport statistics: europa.eu, 2022.

597
598 Alfarrá, M.R., Prevot, A.S., Szidat, S., Sandradewi, J., Weimer, S., Lanz, V.A., Schreiber, D., Mohr, M. and
599 Baltensperger, U.: Identification of the mass spectral signature of organic aerosols from wood burning
600 emissions. *Environmental science & technology*, 41(16), pp.5770-5777, 2007.

601
602 Amato, F., Moreno, T., Pandolfi, M., Querol, X., Alastuey, A., Delgado, A., Pedrero, M. and Cots, N.:
603 Concentrations, sources and geochemistry of airborne particulate matter at a major European airport. *Journal of*
604 *Environmental Monitoring*, 12(4), pp.854-862, <https://doi.org/10.1039/B925439K>, 2010.

605
606 Anderson, B.E., Beyersdorf, A.J., Hudgins, C.H., Plant, J.V., Thornhill, K.L., Winstead, E.L., Ziemba, L.D.,
607 Howard, R., Corporan, E., Miake-Lye, R.C. and Herndon, S.C.: Alternative aviation fuel experiment
608 (AAFEX) (No. NASA/TM-2011-217059), 2011.

609

610 Anderson, B.E., Chen, G. and Blake, D.R.: Hydrocarbon emissions from a modern commercial
611 airliner. *Atmospheric Environment*, 40(19), pp.3601-3612, <https://doi.org/10.1016/j.atmosenv.2005.09.072>,
612 2006.

613
614 Bond, T.C., Streets, D.G., Yarber, K.F., Nelson, S.M., Woo, J.H. and Klimont, Z.: A technology-based global
615 inventory of black and organic carbon emissions from combustion. *Journal of Geophysical Research:*
616 *Atmospheres*, 109(D14), <https://doi.org/10.1029/2003JD003697>, 2004.

617
618 Boldo, E., Medina, S., Le Tertre, A., Hurley, F., Mücke, H.G., Ballester, F., Aguilera, I. and Daniel Eilstein on
619 behalf of the Apheis group.: Apheis: Health impact assessment of long-term exposure to PM 2.5 in 23 European
620 cities. *European journal of epidemiology*, 21, pp.449-458, <https://doi.org/10.1007/s10654-006-9014-0>, 2006.

621
622 Canagaratna, M.R., Jayne, J.T., Jimenez, J.L., Allan, J.D., Alfarra, M.R., Zhang, Q., Onasch, T.B., Drewnick,
623 F., Coe, H., Middlebrook, A. and Delia, A.: Chemical and microphysical characterization of ambient aerosols
624 with the aerodyne aerosol mass spectrometer. *Mass spectrometry reviews*, 26(2), pp.185-222,
625 <https://doi.org/10.1002/mas.20115>, 2007.

626
627 Canonaco, F., Crippa, M., Slowik, J.G., Baltensperger, U. and Prévôt, A.S.: SoFi, an IGOR-based interface for
628 the efficient use of the generalized multilinear engine (ME-2) for the source apportionment: ME-2 application to
629 aerosol mass spectrometer data. *Atmospheric Measurement Techniques*, 6(12), pp.3649-3661,
630 <https://doi.org/10.5194/amt-6-3649-2013>, 2013.

631
632 Carslaw, D.C., Beever, S.D., Ropkins, K. and Bell, M.C.: Detecting and quantifying aircraft and other on-
633 airport contributions to ambient nitrogen oxides in the vicinity of a large international airport. *Atmospheric*
634 *Environment*, 40(28), pp.5424-5434, <https://doi.org/10.1016/j.atmosenv.2006.04.062>, 2006.

635
636 Carslaw, D.C. and Ropkins, K.: Openair—an R package for air quality data analysis. *Environmental Modelling*
637 *& Software*, 27, pp.52-61, <https://doi.org/10.1016/j.envsoft.2011.09.008>, 2012.

638
639 Crilley, L.R., Bloss, W.J., Yin, J., Beddows, D.C., Harrison, R.M., Allan, J.D., Young, D.E., Flynn, M.,
640 Williams, P., Zotter, P. and Prévôt, A.S.: Sources and contributions of wood smoke during winter in London:
641 assessing local and regional influences. *Atmospheric chemistry and physics*, 15(6), pp.3149-3171,
642 <https://doi.org/10.5194/acp-15-3149-2015>, 2015.

643
644 Environmental protection. Annex 16 to the Convention on International Civil Aviation. Volume II aircraft
645 engine emissions. I.C.A.O., 2016.

646
647 Fushimi, A., Saitoh, K., Fujitani, Y. and Takegawa, N.: Identification of jet lubrication oil as a major component
648 of aircraft exhaust nanoparticles. *Atmospheric Chemistry and Physics*, 19(9), pp.6389-6399, 2019.

649
650 He, R.W., Shirmohammadi, F., Gerlofs-Nijland, M.E., Sioutas, C. and Cassee, F.R.: Pro-inflammatory
651 responses to PM_{0.25} from airport and urban traffic emissions. *Science of the total environment*, 640, pp.997-
652 1003, <https://doi.org/10.1016/j.scitotenv.2018.05.382>, 2018.

653
654 Herndon, S.C., Jayne, J.T., Lobo, P., Onasch, T.B., Fleming, G., Hagen, D.E., Whitefield, P.D. and Miake-Lye,
655 R.C.: Commercial aircraft engine emissions characterization of in-use aircraft at Hartsfield-Jackson Atlanta
656 International Airport. *Environmental science & technology*, 42(6), pp.1877-1883,
657 <https://doi.org/10.1021/es072029+>, 2008.

658
659 Helin, A., Niemi, J.V., Virkkula, A., Pirjola, L., Teinilä, K., Backman, J., Aurela, M., Saarikoski, S., Rönkkö,
660 T., Asmi, E. and Timonen, H.: Characteristics and source apportionment of black carbon in the Helsinki
661 metropolitan area, Finland. *Atmospheric Environment*, 190, pp.87-98,
662 <https://doi.org/10.1016/j.atmosenv.2018.07.022>, 2018.

663
664 Hu, S., Fruin, S., Kozawa, K., Mara, S., Winer, A.M. and Paulson, S.E.: Aircraft emission impacts in a
665 neighborhood adjacent to a general aviation airport in Southern California. *Environmental science &*
666 *technology*, 43(21), pp.8039-8045, <https://doi.org/10.1021/es900975f>, 2009.

667

668 Hudda, N. and Fruin, S.A.: International airport impacts to air quality: size and related properties of large
669 increases in ultrafine particle number concentrations. *Environmental science & technology*, 50(7), pp.3362-
670 3370, <https://doi.org/10.1021/acs.est.5b05313>, 2016.
671

672 Hudda, N., Gould, T., Hartin, K., Larson, T.V. and Fruin, S.A.: Emissions from an international airport increase
673 particle number concentrations 4-fold at 10 km downwind. *Environmental science & technology*, 48(12),
674 pp.6628-6635, <https://doi.org/10.1021/es5001566>, 2014.
675

676 Hudda, N., Simon, M.C., Zamore, W., Brugge, D. and Durant, J.L.: Aviation emissions impact ambient ultrafine
677 particle concentrations in the greater Boston area. *Environmental science & technology*, 50(16), pp.8514-8521,
678 <https://doi.org/10.1021/acs.est.6b01815>, 2016.
679

680 Jimenez, J.L., Canagaratna, M.R., Donahue, N.M., Prevot, A.S.H., Zhang, Q., Kroll, J.H., DeCarlo, P.F., Allan,
681 J.D., Coe, H., Ng, N.L. and Aiken, A.C.: Evolution of organic aerosols in the atmosphere. *Science*, 326(5959),
682 pp.1525-1529, <https://doi.org/10.1126/science.118035>, 2009.
683

684 Jonsdottir, H.R., Delaval, M., Leni, Z., Keller, A., Brem, B.T., Siegerist, F., Schönenberger, D., Durdina, L.,
685 Elser, M., Burtscher, H. and Liati, A.: Non-volatile particle emissions from aircraft turbine engines at ground-
686 idle induce oxidative stress in bronchial cells. *Communications biology*, 2(1), p.90,
687 <https://doi.org/10.1038/s42003-019-0332-7>, 2019.
688

689 Kinsey, J.S.: Characterization of emissions from commercial aircraft engines during the Aircraft Particle
690 Emissions eXperiment (APEX) 1 to 3. Office of Research and Development, US Environmental Protection
691 Agency, 2009.
692

693 Kinsey, J.S., Dong, Y., Williams, D.C. and Logan, R.: Physical characterization of the fine particle emissions
694 from commercial aircraft engines during the Aircraft Particle Emissions eXperiment (APEX) 1–3. *Atmospheric*
695 *Environment*, 44(17), pp.2147-2156, <https://doi.org/10.1016/j.atmosenv.2010.02.010>, 2010.
696

697 Kinsey, J.S., Hays, M.D., Dong, Y., Williams, D.C. and Logan, R.: Chemical characterization of the fine
698 particle emissions from commercial aircraft engines during the Aircraft Particle Emissions eXperiment (APEX)
699 1 to 3. *Environmental science & technology*, 45(8), pp.3415-3421, <https://doi.org/10.1021/es103880d>, 2011.
700

701 Lee, D.S., Pitari, G., Grewe, V., Gierens, K., Penner, J.E., Petzold, A., Prather, M.J., Schumann, U., Bais, A.,
702 Bernsten, T. and Iachetti, D.: Transport impacts on atmosphere and climate: Aviation. *Atmospheric*
703 *environment*, 44(37), pp.4678-4734, <https://doi.org/10.1016/j.atmosenv.2009.06.005>, 2010.
704

705 Li, N., Hao, M., Phalen, R.F., Hinds, W.C. and Nel, A.E.: Particulate air pollutants and asthma: a paradigm for
706 the role of oxidative stress in PM-induced adverse health effects. *Clinical immunology*, 109(3), pp.250-265,
707 <https://doi.org/10.1016/j.clim.2003.08.006>, 2003.

708 Liu, G., Yan, B. and Chen, G.: Technical review on jet fuel production. *Renewable and Sustainable Energy*
709 *Reviews*, 25, pp.59-70, 2013.

710 Masiol, M. and Harrison, R.M.: Aircraft engine exhaust emissions and other airport-related contributions to
711 ambient air pollution: A review. *Atmospheric Environment*, 95, pp.409-455,
712 <https://doi.org/10.1016/j.atmosenv.2014.05.070>, 2014.
713

714 Mazaheri, M., Johnson, G.R. and Morawska, L.: An inventory of particle and gaseous emissions from large
715 aircraft thrust engine operations at an airport. *Atmospheric Environment*, 45(20), pp.3500-3507,
716 <https://doi.org/10.1016/j.atmosenv.2010.12.012>, 2011.
717

718 NIST Mass Spectrometry Data Center. Decane, US secretary of commerce.
719 <https://webbook.nist.gov/cgi/cbook.cgi?ID=C124185&Mask=200#Mass-Spec>, 1990.
720

721 Onasch, T.B., Jayne, J.T., Herndon, S., Worsnop, D.R., Miake-Lye, R.C., Mortimer, I.P. and Anderson, B.E.:
722 Chemical properties of aircraft engine particulate exhaust emissions. *Journal of Propulsion and Power*, 25(5),
723 pp.1121-1137, <https://doi.org/10.2514/1.36371>, 2009.
724

725 Paatero, P.: The multilinear engine—a table-driven, least squares program for solving multilinear problems,
726 including the n-way parallel factor analysis model. *Journal of Computational and Graphical Statistics*, 8(4),
727 pp.854-888, <https://doi.org/10.1080/10618600.1999.10474853>, 1999.

728 Paatero, P. and Tapper, U.: Positive matrix factorization: A non-negative factor model with optimal utilization
729 of error estimates of data values. *Environmetrics*, 5(2), pp.111-126, <https://doi.org/10.1002/env.3170050203>,
730 1994.

731
732 Petzold, A. and Schönlinner, M.: Multi-angle absorption photometry—a new method for the measurement of
733 aerosol light absorption and atmospheric black carbon. *Journal of Aerosol Science*, 35(4), pp.421-441,
734 <https://doi.org/10.1016/j.jaerosci.2003.09.005>, 2004.

735
736 Pope III, C.A. and Dockery, D.W.: Health effects of fine particulate air pollution: lines that connect. *Journal of*
737 *the air & waste management association*, 56(6), pp.709-742, <https://doi.org/10.1080/10473289.2006.10464485>,
738 2006.

739 Reyes-Villegas, E., Green, D.C., Priestman, M., Canonaco, F., Coe, H., Prévôt, A.S. and Allan, J.D.: Organic
740 aerosol source apportionment in London 2013 with ME-2: exploring the solution space with annual and seasonal
741 analysis. *Atmospheric Chemistry and Physics*, 16(24), pp.15545-15559, [https://doi.org/10.5194/acp-16-15545-](https://doi.org/10.5194/acp-16-15545-2016)
742 2016, 2016.

743
744 Reyes-Villegas, E., Priestley, M., Ting, Y.C., Haslett, S., Bannan, T., Le Breton, M., Williams, P.I., Bacak, A.,
745 Flynn, M.J., Coe, H. and Percival, C.: Simultaneous aerosol mass spectrometry and chemical ionisation mass
746 spectrometry measurements during a biomass burning event in the UK: insights into nitrate
747 chemistry. *Atmospheric Chemistry and Physics*, 18(6), pp.4093-4111, [https://doi.org/10.5194/acp-18-4093-](https://doi.org/10.5194/acp-18-4093-2018)
748 2018, 2018.

749
750 Rissman, J., Arunachalam, S., Woody, M., West, J.J., BenDor, T. and Binkowski, F.S.: A plume-in-grid
751 approach to characterize air quality impacts of aircraft emissions at the Hartsfield–Jackson Atlanta International
752 Airport. *Atmospheric Chemistry and Physics*, 13(18), pp.9285-9302, <https://doi.org/10.5194/acp-13-9285-2013>,
753 2013.

754
755 Salihu, A.L., Lloyd, S.M. and Akgunduz, A.: Electrification of airport taxiway operations: A simulation
756 framework for analyzing congestion and cost. *Transportation Research Part D: Transport and Environment*, 97,
757 p.102962, <https://doi.org/10.1016/j.trd.2021.102962>, 2021.

758
759 Schripp, T., Anderson, B.E., Bauder, U., Rauch, B., Corbin, J.C., Smallwood, G.J., Lobo, P., Crosbie, E.C.,
760 Shook, M.A., Miake-Lye, R.C. and Yu, Z.: Aircraft engine particulate matter emissions from sustainable
761 aviation fuels: Results from ground-based measurements during the NASA/DLR campaign ECLIF2/ND-
762 MAX. *Fuel*, 325, p.124764, <https://doi.org/10.1016/j.fuel.2022.124764>, 2022.

763
764 Schwarze, P.E., Øvreivik, J., Låg, M., Refsnes, M., Nafstad, P., Hetland, R.B. and Dybing, E.: Particulate matter
765 properties and health effects: consistency of epidemiological and toxicological studies. *Human & experimental*
766 *toxicology*, 25(10), pp.559-579, <https://doi.org/10.1177/096032706072520>, 2006.

767
768 Smith, L.D., Allan, J., Coe, H., Reyes-Villegas, E., Johnson, M.P., Crayford, A., Durand, E. and Williams, P.I.:
769 Examining chemical composition of gas turbine-emitted organic aerosol using positive matrix factorisation
770 (PMF). *Journal of Aerosol Science*, 159, p.105869, <https://doi.org/10.1016/j.jaerosci.2021.105869>, 2022.

771
772 Stettler, M.E.J., Eastham, S. and Barrett, S.R.H.: Air quality and public health impacts of UK airports. Part I:
773 Emissions. *Atmospheric environment*, 45(31), pp.5415-5424, <https://doi.org/10.1016/j.atmosenv.2011.07.012>,
774 2011.

775
776 Timko, M.T., Albo, S.E., Onasch, T.B., Fortner, E.C., Yu, Z., Miake-Lye, R.C., Canagaratna, M.R., Ng, N.L.
777 and Worsnop, D.R.: Composition and sources of the organic particle emissions from aircraft engines. *Aerosol*
778 *Science and Technology*, 48(1), pp.61-73, <https://doi.org/10.1080/02786826.2013.857758>, 2014.

779

780 Timko, M.T., Onasch, T.B., Northway, M.J., Jayne, J.T., Canagaratna, M.R., Herndon, S.C., Wood, E.C.,
781 Miake-Lye, R.C. and Knighton, W.B.: Gas turbine engine emissions—Part II: chemical properties of particulate
782 matter. <https://doi.org/10.1115/1.4000132>, 2010.
783

784 Ulbrich, I.M., Canagaratna, M.R., Zhang, Q., Worsnop, D.R. and Jimenez, J.L.: Interpretation of organic
785 components from Positive Matrix Factorization of aerosol mass spectrometric data. *Atmospheric Chemistry and
786 Physics*, 9(9), pp.2891-2918, <https://doi.org/10.5194/acp-9-2891-2009>, 2009.
787

788 Ungeheuer, F., Caudillo, L., Ditas, F., Simon, M., van Pinxteren, D., Kılıç, D., Rose, D., Jacobi, S., Kürten, A.,
789 Curtius, J. and Vogel, A.L.: Nucleation of jet engine oil vapours is a large source of aviation-related ultrafine
790 particles. *Communications Earth & Environment*, 3(1), p.319, <https://doi.org/10.1038/s43247-022-00653-w>,
791 2022.
792

793 van Baaren, E.: The feasibility of a fully electric aircraft towing system. 2019.
794

795 Westerdaal, D., Fruin, S.A., Fine, P.L. and Sioutas, C.: The Los Angeles International Airport as a source of
796 ultrafine particles and other pollutants to nearby communities. *Atmospheric Environment*, 42(13), pp.3143-
797 3155, <https://doi.org/10.1016/j.atmosenv.2007.09.006>, 2008.
798

799 Yang, X., Cheng, S., Lang, J., Xu, R. and Lv, Z.: Characterization of aircraft emissions and air quality impacts
800 of an international airport. *Journal of environmental sciences*, 72, pp.198-207,
801 <https://doi.org/10.1016/j.jes.2018.01.007>, 2018.
802

803 Yim, S.H., Stettler, M.E. and Barrett, S.R.: Air quality and public health impacts of UK airports. Part II: Impacts
804 and policy assessment. *Atmospheric environment*, 67, pp.184-192,
805 <https://doi.org/10.1016/j.atmosenv.2012.10.017>, 2013.
806

807 Yu, K.N., Cheung, Y.P., Cheung, T. and Henry, R.C.: Identifying the impact of large urban airports on local air
808 quality by nonparametric regression. *Atmospheric Environment*, 38(27), pp.4501-4507,
809 <https://doi.org/10.1016/j.atmosenv.2004.05.034>, 2004.
810

811 Yu, Z., Herndon, S.C., Ziemba, L.D., Timko, M.T., Liscinsky, D.S., Anderson, B.E. and Miake-Lye, R.C.:
812 Identification of lubrication oil in the particulate matter emissions from engine exhaust of in-service commercial
813 aircraft. *Environmental science & technology*, 46(17), pp.9630-9637, <https://doi.org/10.1021/es301692t>, 2012.
814

815 Yu, Z., Liscinsky, D.S., Winstead, E.L., True, B.S., Timko, M.T., Bhargava, A., Herndon, S.C., Miake-Lye,
816 R.C. and Anderson, B.E.: Characterization of lubrication oil emissions from aircraft engines. *Environmental
817 science & technology*, 44(24), pp.9530-9534, <https://doi.org/10.1021/es102145z>, 2010.
818

819 Yu, Z., Timko, M.T., Herndon, S.C., Richard, C., Beyersdorf, A.J., Ziemba, L.D., Winstead, E.L. and Anderson,
820 B.E.: Mode-specific, semi-volatile chemical composition of particulate matter emissions from a commercial gas
821 turbine aircraft engine. *Atmospheric Environment*, 218, p.116974,
822 <https://doi.org/10.1016/j.atmosenv.2019.116974>, 2019.
823

824 Yunos, S.N.M.M., Ghafir, M.F.A. and Wahab, A.A.: April. Aircraft LTO emissions regulations and
825 implementations at European airports. In *AIP Conference Proceedings* (Vol. 1831, No. 1),
826 <https://doi.org/10.1063/1.4981147>, 2017.
827

828 Zhang, Q., Jimenez, J.L., Canagaratna, M.R., Allan, J.D., Coe, H., Ulbrich, I., Alfarra, M.R., Takami, A.,
829 Middlebrook, A.M., Sun, Y.L. and Dzepina, K.: Ubiquity and dominance of oxygenated species in organic
830 aerosols in anthropogenically-influenced Northern Hemisphere midlatitudes. *Geophysical research
831 letters*, 34(13), <https://doi.org/10.1029/2007GL029979>, 2007.
832

833 Zhu, Y., Fanning, E., Yu, R.C., Zhang, Q. and Froines, J.R.: Aircraft emissions and local air quality impacts
834 from takeoff activities at a large International Airport. *Atmospheric Environment*, 45(36), pp.6526-6533,
835 <https://doi.org/10.1016/j.atmosenv.2011.08.062>, 2011.
836
837
838
839

840
841